



Short Convergence Time Super-Twisting Sliding Mode Speed Control of Permanent Magnet Synchronous Motor

Fuat KILIÇ^{1,*} ¹ Department of Electrical&Electronics Engineering, Balıkesir University, Balıkesir, Türkiye, **ORCID:** 0000-0003-2502-3789

Article Info

Research paper

Received : September 3, 2024

Accepted : October 13, 2024

Keywords

Permanent Magnet Synchronous Motor
Super Twisting Method
Sliding Mode Control
Robust Control

Abstract

One of the most popular motors for precise control applications, such as electric vehicles, is the permanent magnet synchronous motor (PMSM). Under harsh conditions, PMSM and its drives are expected to provide robust control response against internal and external disturbances. Conventional controllers used in the vector control method have difficulty providing superior control responses due to the nonlinear structure of the PMSM. Although sliding mode control is a good control method to fulfill these control requirements, it has a chattering effect due to high-speed switching phenomenon. To reduce this effect and to obtain a better dynamic response, super-twisting sliding mode control (ST-SMC) is one of the control method candidates. In the classical ST-SMC control method, since the sliding surface consists of error or error-integral of the error, the finite time convergence to the equilibrium point is not fast enough. In this study, a new nonlinear sliding surface is designed in the ST-SMC controller for speed control of PMSM. In addition, equivalent control terms and an error-dependent exponential term are added to the control input to speed up the output response. In this way, the ST-SMC algorithm is experimentally applied to control the speed of the PMSM under harsh operating conditions with reduced chattering, shortened convergence time, and increased robustness against internal and external disturbances. The experimental implementation of the designed controller is carried out on a 400 W PMSM motor test setup. The superiority of the proposed control algorithm is comparatively demonstrated under operating conditions such as step speed reference and load torque.

1. Introduction

The environment, exposed to greenhouse gas emissions from past to present, continues to be increasingly polluted. This is why there is an increasing interest in electric vehicles, which are becoming more and more commonplace and accelerating quickly [1-4]. Electric vehicles can contribute significantly to the reduction of greenhouse gas due to their zero emissions, superior efficiency and other energy-saving capacities compared to internal combustion engines (ICE). In addition to these positive aspects of electric vehicles, driving comfort also seems to cause people to prefer them more. The motor is one of the most important components of electric vehicle drive system, which determines the high dynamic performance of the vehicle. Since they are small and highly efficient, permanent magnet synchronous machines,

or PMSMs, are frequently utilized in industrial settings, including electric cars and lifts [5,6]. Because PMSMs are widely used in commercial and industrial applications, precise knowledge of the machine's specifications is essential for dependable, high-performance control.

Field-oriented vector control method maintains its place as the most important method shaping the driving comfort of electric vehicles. When choosing an electric vehicle, drivers give significant priority to driving performance. The physical state of the road and the volume of traffic are two examples of the conditions in which driving performance is evaluated [7]. Maneuvers like stop-and-go, abrupt acceleration, and quick stops are the best ways to assess driving performance in these difficult circumstances. PMSM and its drives are projected to exhibit improved dynamic response and robust control response to disturbances under these test settings [8]. Conventional controller used in the vector control method makes it difficult to fulfill the superior control requirements of PMSM due to its multivariable structure,

* Corresponding Author: fuatkilic@balikesir.edu.tr



strong coupling and nonlinear structure [9]. Within the PMSM drive speed loop, PI controllers are among the most used techniques [10]. Pole-zero cancellation method with linear control theory allows speed to be regulated in the transfer function without permanent error [11]. With regard to this method, pole-zero cancellation depends on the accuracy of the motor model. In cases where precise control is required, the motor will be subject to two-way disturbances. Internal disturbances resulting from motor parameter ambiguity are the first of these [12]. Internal degradations are brought on by variations in motor resistance and inductance as a result of saturation and outside temperature. Because of this, it is challenging to use a PI controller to control PMSM and achieve a strong control structure. Other disturbances are external disturbances caused by load torque and instantaneous operating conditions in the speed control loop of the motor [13]. If a speed controller cannot provide a control signal that is robust against external disturbances, speed reference cannot be tracked accurately and precisely. This leads to a decrease in the control quality. For this purpose, many controller methods have been proposed to cope with the nonlinear structure of PMSM. Among them are feedback linearization control, active disturbance rejection control (ADRC) [14], backstepping control [15], sliding mode control (SMC) [16], fuzzy control [17], and model predictive control (MPC) [18] and so on.

Among these methods, nonlinear sliding mode control (SMC) is the most well-known method that can provide robust control output against the challenging nature and uncertainties of PMSM. One of the prominent features of SMC is its robust control response to uncertainties [19]. To strengthen control of speed loop robustness against both internal and external disturbances, a sliding mode controller has been suggested [13]. The high-frequency switching structure in this control system creates a problem with chattering that needs to be resolved. A boundary layer-based chattering reduction technique in first-order sliding mode control has been developed for this reason [20]. However, this strategy sacrifices the robustness of the regulator in order to decrease chattering. Furthermore, control systems often have steady-state errors as a result [21]. The chattering issue can be minimized by creating a suitable sliding surface-reaching law, as it stems from inadequate convergence to the sliding surface. It is developed and experimented with an adaptive terminal sliding mode reaching law [22]. The findings show that there is less chattering and an improvement in control sensitivity. A sliding mode reaching law that is robust to disturbances is designed in [23] and can offer a good speed transient response that includes power term and system state variable. The sign function is substituted by the hyperbolic tangent function in [24]. The performance of

the control is enhanced, and the chattering effect is lessened. An exponential function and a system state variable are added in [25], which is based on the classical power-reaching law. By doing this, they demonstrated how chattering is effectively alleviated and reaching time is shortened. However, six parameters need to be changed to reach the law to lessen chattering. In this case, the control structure is more complex. Thus, the suggested reaching law ought to lessen chattering, speed up convergence, avoid complicating the control structure, and aid in the reduction of number of the parameters. Terminal sliding mode (TSM) is a commonly employed method in PMSM systems designed to accelerate the convergence to the sliding surface. Although it avoids the singularity issue in TSM and offers faster finite-time convergence than TSM, fast non-singular TSM (FNTSM) control still has a discontinuous control law problem. Continuous non-singular fast TSM (CFNTSM) control has been developed and effectively applied in the PMSM system to address the chattering issue brought about by the discontinuous control rule in FNTSM control schemes [26]. However, the robustness and dynamic response of the controller still need to be improved for practical applications. In addition to these methods, a second-order SMC (SO-SMC) based on FO-SMC has been proposed by Levant [27]. In this method, the cracking resulting from high-frequency switching control can be reduced by deriving the sliding surface. The steady-state error at the controller output is resolved by driving the sliding mode variable and its first derivative to zero within a finite time [28].

The super-twisting sliding mode control (ST-SMC), which is a typical SO-SMC, is easily applicable and particularly suitable for first-order systems. Therefore, it has been proposed to enhance the robustness in the control of motor drives using ST-SMC and in [29] ST-SMC has been applied as a controller that enhances robustness in transient changes of speed and torque parameters in the direct torque control of AC motors. In [30], it has been noted that although the performance of the control system is enhanced by ST-SMC, the necessary response to time-varying external disturbances is not fully demonstrated. Hence, a variable gain ST-SMC is proposed to provide global bounded-time convergence against disturbances. Two functions are utilized to bind the disturbances, assuming the disturbance boundaries are known. However, it is challenging to calculate or estimate disturbances in motor speed control. In [31], observer-based controllers are proposed to counteract disturbances that may occur in the ST-SMC system. However, this approach increases complexity. [32] focus on redesigning the sliding surface to achieve a robust control response against known and unknown disturbances. In this study, to enhance control performance against disturbances, the method relies on

increasing the integral gain, leading to overshoot and oscillations in the control response.

This study investigates the experimental implementation of a nonlinear sliding surface to enhance the robustness against internal and external disturbances experienced during the operation of Permanent Magnet Synchronous Motors (PMSMs) used in electric vehicle applications and similar domains, aiming to shorten the convergence time of bounded-time convergence when considering the sliding surface variable as the error.

2. Materials and Methods

In this section, the mathematical model of PMSM, first-order sliding mode control, the proposed method and stability analysis, and finally the experimental setup will be presented respectively.

2.1. Mathematical Model of The PMSM

In the rotor $d - q$ reference frame, the mathematical model of the PMSM system is represented as follows:

$$\frac{di_d}{dt} = \frac{1}{L_d}(-Ri_d + P\omega_m L_q i_q + v_d) \quad (1)$$

$$\frac{di_q}{dt} = \frac{1}{L_q}(-Ri_q - P\omega_m L_q i_q - P\omega_m \Phi + v_q) \quad (2)$$

$$T_e = 1.5P[\Phi i_q + (L_d - L_q)i_d i_q] \quad (3)$$

where the stator voltage and current in the d -axis are represented by v_d , and i_d respectively, and the stator voltage and current in the q -axis are by v_q and i_q . The stator resistance is denoted by R , rotor pole pairs is P , the flux linkage value of the rotor permanent magnets is represented by λ_m ; the mechanical speed of the rotor is represented by ω_m the electromagnetic torque is represented by T_e . The PMSM's constant flux condition was achieved by setting the d -axis target value to zero and treating the d - and q -axis inductances as equivalent, as stated in. The q -axis current is the only factor that affects the electromagnetic torque, T_e , which has the following expression:

$$T_e = \frac{3}{2}P\lambda_m i_q = K_t i_q \quad (4)$$

In this situation, K_t represents the torque constant. The equation describing the rotation of the motor can be expressed as:

$$\frac{d\theta_e}{dt} = \omega_e \quad (5)$$

$$T_e = J \frac{d\omega}{dt} + B\omega + T_L \quad (6)$$

where ω_e the electrical angular velocity, θ_e denotes the electrical rotor's position angle, J stands for the load and rotor combined moment of inertia, B is the frictional coefficient, and T_L is the assumed external load torque, which varies gradually over a short sampling interval.

$$T_e = J_n \frac{d\omega_m}{dt} + B_n \omega_m + d \quad (7)$$

where J_n and B_n represent J and B 's nominal values, respectively, with $J = J_n + \Delta J, B = B_n + \Delta B$. d value is

described as $d = \Delta J \frac{d\omega_m}{dt} + \Delta B \omega_m + T_L$ which includes motor

parameter changes and load torque. These are counted as lumped disturbances in the system. The uncertain value of d leads to lumped disturbances in the system, which in turn causes an undesirable dynamic response. 1) The lumped disturbances are bound (that is, $|d| < D_1$ with $D_1 > 0$) and vary slowly over a brief sample time in the real system. They do not have an overwhelming impact on the system. 2) There exists $D_2 > 0$ such that $|d| < D_2$, thereby binding the disturbance derivative in the controller as well.

2.2. First Order Sliding Mode (FO-SMC) Controller Design

Sliding Mode Control (SMC) exhibits a stronger resistance to variations in internal values and external disturbances compared to other nonlinear control approaches, providing the system trajectory hits and stays on the sliding surface. The initial stage in implementing a speed controller that utilizes sliding mode control is the selection of the sliding-mode surface. The following stage involves arranging the control input in such a way that the system motion is steered towards the sliding-mode surface, ensuring that the system meets the sliding-mode reaching criterion. The system is characterized by a comprehensive nonlinear model, which is regarded as

$$\begin{aligned} \dot{x}_1 &= x_2 \\ \dot{x}_2 &= f(x) + g(x) + b(x)u \end{aligned} \quad (8)$$

The system state vector is denoted by x , the input matrix is $b(x)$, the control input is u , and system disturbances are represented by $g(x)$. Sliding control input includes two parts. Equivalent control and switching control are parts that form total control law. SMC control law is designed as Eq. 9

$$u_c = u_{eq} + u_{sw} \quad (9)$$

where u_c is the equivalent control term, u_{sw} is the switching term and u_c is the total control term. The objective of the control is to accurately follow the desired speed and minimize any deviation between the desired speed and the actual speed of the rotor. Speed Error between reference speed and actual speed is expressed Eq. 10. The speed error is selected as sliding surface. The sliding surface is derivated to

$$s = e_s = \omega_{ref} - \omega_m \quad (10)$$

$$\dot{s} = \dot{e}_s = \dot{\omega}_{ref} - \dot{\omega}_m \quad (11)$$

The PMSM speed control loop is presented as first-order system. Conventional FO-SMC control is designed for sliding surface and its derivative.

$$\dot{s} = \dot{\omega}_{ref} - \left(\frac{T_e}{J} - \frac{B\omega_m}{J} - \frac{T_l}{J} \right) \quad (12)$$

s and \dot{s} sliding surface and its derivative in sliding mode is to force go to zero as control objective. When the sliding surface derivative is zero, Eq.13 is as follows. In this case, the solution of the control vector is expressed as equivalent control.

$$\dot{\omega}_{ref} - \frac{3P\lambda_m}{2J} I_q + \frac{B}{J} \omega_m + \frac{T_l}{J} = 0 \quad (13)$$

$$I_q = \frac{2J}{3P\lambda_m} \left[\dot{\omega}_{ref} + \frac{B}{J} \omega_m + \frac{T_l}{J} \right] \quad (14)$$

Switching function is comprised of the sign function. Sign function is written as Eq. 15.

$$\text{sgn}(s) = \begin{cases} 1 & s > 0 \\ 0 & s = 0 \\ -1 & s < 0 \end{cases}, \quad (15)$$

Finally reference q-axis current is defined as Eq.16

$$i_q^* = \frac{2J}{3P\lambda_m} \left[\dot{\omega}_{ref} - \frac{B}{J} \omega_m \right] + K \text{sgn}(s) \quad (16)$$

where K is constant that establishes stability of control system. Substituting i_q^* into Eq.10,

$$\dot{s} = -K_t \text{sgn}(s) \quad (17)$$

sliding surface derivative is obtained. The stability condition is based on a quadratic Lyapunov function like $V = \frac{1}{2} s^2$. The Lyapunov function candidate must have a positive value and its derivate negative value. The Lyapunov function derivative is given in Eq. 18.

$$\dot{V} = s\dot{s} < 0 \quad \forall s \quad (18)$$

$K_t = \frac{3P\lambda_m}{2J} K$ gain is total gain. Hence, stability condition is written as Eq. 19.

$$\dot{V} = s(-K_t \text{sgn}(s)) \quad (19)$$

$$\dot{V} = -K_t |s| \quad (20)$$

If $K_t > 0$ in Eq. 20 guarantees that $\dot{V} < 0$ or negative definite. As a result, stability condition is fulfilled.

2.3. Short Convergence Time Super-Twisting Sliding Mode Controller (SCTST-SMC)

The tradeoff between chattering and convergence rate at the same time cannot be resolved by traditional SMC. While a big sliding mode gain can ensure a sufficient convergence rate, it also causes significant chattering and compromises the stability of the system. Small sliding mode gain, on the other hand, can reduce chattering but slows down the system's tracking reaction. The switching function is included in the integral term of second-order SMC since it is the primary cause of sliding mode chattering. The filtering characteristic of the integral can be used to efficiently alleviate chattering. By calculating the n time derivatives of the sliding variable s , $[\dot{s}, \ddot{s}, \dots, s^{(n)}]$ can be obtained. The derivative order of s with a "sliding discontinuity" (such as the sign function) is defined as the sliding order. Another expression is the relative degree that is aspects of the system control. The following relationship is found by calculating the Lie Derivatives regarding the output $h(x, t)$ function

$$\frac{d(L_f^{n-1} h(x))}{dt} = L_f^n h(x) + L_g L_f^{n-1} h(x) u \quad (21)$$

A relative degree can be defined as the first n values of time derivatives of the outputs $[h, \dot{h}, \dots, h^{(n)}]$ where u namely control input appears explicitly. A first-order sliding mode leads s to drive to zero but not its derivative \dot{s} , resulting in the chattering where the sliding variables oscillate very close to zero. ST-SMC is the most powerful method for second-order continuous sliding mode control. When provided with a certain limit and smooth perturbations that have a defined gradient, this system generates a continuous control function that causes the sliding variable and its derivative to reach zero within a specified amount of time. Chattering is reduced rather than eliminated because the ST-SMC is integrated and has a discontinuous function [33]. STA applies to a system (generally any order) where control appears in the first derivative of the sliding surface, in contrast to conventional second-order sliding mode controllers [31]. The STA was first presented in [27] as:

$$\begin{aligned} u &= -K_1 |\sigma|^{1/2} \text{sgn}(\sigma) + \nu \\ \dot{\nu} &= -K_2 \text{sgn}(\sigma) \end{aligned} \quad (22)$$

where K_i are gains to be estimated. If the input signal $f(t)$ is a bounded function and composed of a base signal with a derivative with the Lipschitz constant $C > 0$. Consequently, adequate conditions for the convergences of $s, \dot{s} = 0$ is

$$K_2 > C, \quad K_1^2 \geq 4C \frac{K_2 + C}{K_2 - C} \quad (23)$$

The conditions in Eq. 23 result from a very rough estimate. Calculations show that many other values can be taken, such as $K_1 = 1.5C, K_2 = 1.1C$. PMSM speed sliding surface is addressed to control before and conventional super twisting control involves linear terms in its sliding surface. Time derivations of speed control are expressed as

$$\begin{cases} x_1 = e_s = \omega_{ref} - \omega_m \\ x_2 = \dot{x}_1 = \dot{\omega}_{ref} - \dot{\omega}_m \end{cases} \quad (24)$$

$$\begin{cases} \dot{x}_1 = \dot{\omega}_{ref} - \dot{\omega}_r = \dot{\omega}_{ref} - \frac{3P\lambda_m}{2J} i_q + \frac{B}{J} \omega_m + \frac{T_l}{J} \\ \dot{x}_2 = \ddot{\omega}_{ref} - \ddot{\omega}_r = \ddot{\omega}_{ref} - \frac{3P\lambda_m}{2J} \frac{di_q}{dt} + \frac{B}{J} \dot{\omega}_m - \frac{\dot{T}_l}{J} \end{cases} \quad (25)$$

The terminal sliding mode surface like is adapted to the sliding mode surface to improve the speed response and increase the convergence speed and is defined as Eq.26

$$s = e + \alpha_1 \int e_s + \alpha_2 e_s^\beta \quad (26)$$

$$\dot{s} = \dot{e}_s + \alpha_1 e_s + \alpha_2 \beta e_s^{\beta-1} \dot{e}_s \quad (27)$$

Where $\alpha_1, \alpha_2, \beta$ are positive constants and β is chosen as $\frac{p_1}{q_1}$. p_1 and p_2 are odd positive numbers. u_{eq} equivalent control component is introduced with ST-SMC sliding surface modification in total control input. Finally, The switching control input ensures that the sliding mode surface is reached, while the equivalent control input ensures that the state variable remains on the surface. Equivalent control input is defined as follows.

$$u_{eq} = \dot{\omega}_r^{ref} + \alpha_1 e_s + \alpha_2 e_s^\beta \quad (28)$$

Switching function is redefined as

$$\begin{aligned} u_{sw} &= -\lambda_1 |e_s|^{1/2} \text{sgn}(e_s) - \lambda_2 e_s + \nu \\ \dot{\nu} &= -\lambda_3 \text{sign}(e_s) - \lambda_4 e_s \end{aligned} \quad (29)$$

Where K_1, K_2, τ_1, τ_2 are positive constants. Total control input is sum of switching function and equivalent control.

$$u_t = \frac{J}{Kt} (u_{eq} + u_{sw}) \quad (30)$$

$$\begin{aligned} i_q^{ref} &= \frac{J}{K_t} (\dot{\omega}_{ref} + \frac{B}{J} \omega_m + \frac{T_l}{J} - \lambda_1 |e_s|^{1/2} \text{sgn}(e_s) - \lambda_2 e_s \\ &\quad - \lambda_3 \text{sign}(e_s) - \lambda_4 e_s) \end{aligned} \quad (31)$$

The design of total control input leads to improve dynamic control response for the reasons given below:

1. There is much less chattering since the discontinuous sign term is included in the integral. The controller design is made simpler by the super-twisting algorithm as compared to the current second-order sliding mode techniques. This is because it needs fewer parameters.
2. Sliding surface involves exponential term that accelerates convergence speed to tend zero.
3. Compared to the traditional ST-SMC algorithm, the proposed algorithm adds $\lambda_2 e_s$ terms to the control input. The $\lambda_2 e_s$ term accelerates the control response and $\lambda_4 e_s$ reduces the overshoot.

2.3.1. Stability Analysis

Stability analysis is made based on quadratic Lyapunov functions. The function has to be a global asymptotic feature [34]. According to these conditions, the

function is defined as follows

$$V(x) = 2\lambda_3|x_1| + \lambda_4x_1^2 + \frac{1}{2}x_2^2 + \frac{1}{2}(\lambda_1|x_1|^{1/2} \text{sign}(x_1) + \lambda_2x_1 - x_2)^2 \quad (32)$$

The Lyapunov function is expressed as quadratic form

$$V(x) = \psi^T \Pi \psi \quad (33)$$

$$\psi = \begin{bmatrix} |x_1|^{1/2} \text{sign}(x_1) \\ x_1 \\ x_2 \end{bmatrix}, \quad \Pi = \frac{1}{2} \begin{bmatrix} (4\lambda_3 + \lambda_1^2) & \lambda_1\lambda_2 & -\lambda_1 \\ \lambda_1\lambda_2 & (2\lambda_4 + \lambda_2^2) & \lambda_2 \\ -\lambda_1 & \lambda_2 & 2 \end{bmatrix} \quad (34)$$

Time derivative of the Lyapunov function is taken as

$$\dot{V} = -\frac{1}{|x_1|^{1/2}} \psi^T \Pi_1 \psi - \psi^T \Pi_2 \psi \quad (35)$$

$$\Pi_1 = \frac{\lambda_1}{2} \begin{bmatrix} (2\lambda_3 + \lambda_1^2) & 0 & -\lambda_1 \\ 0 & (2\lambda_4 + 5\lambda_2^2) & -3\lambda_2 \\ -\lambda_1 & -3\lambda_2 & 1 \end{bmatrix}, \quad \Pi_2 = \lambda_2 \begin{bmatrix} (\lambda_3 + 2\lambda_1^2) & 0 & 0 \\ 0 & (\lambda_4 + \lambda_2^2) & -\lambda_2 \\ 0 & -\lambda_2 & 1 \end{bmatrix} \quad (36)$$

$$\dot{V} \leq -\gamma_1 V^{1/2} - \gamma_2 V \quad (37)$$

Where γ_1, γ_2 are constants of negative definite the Lyapunov function derivative and are determined from Lyapunov function matrix eigenvalues.

$$\gamma_1 = \frac{\phi_{\min}^{1/2}\{\Pi\} \phi_{\min}\{\Pi_1\}}{\phi_{\max}\{\Pi\}}, \gamma_2 = \frac{\phi_{\min}\{\Pi_2\}}{\phi_{\max}\{\Pi\}} \quad (38)$$

Under the above conditions, ST-SMC controller gains are selected as

$$\begin{cases} \lambda_1 > 2\eta_1^2 \\ \lambda_2 > \frac{(2\eta_1)^{1/2}}{2} \\ \lambda_3 > \eta_1 \\ \lambda_4 > \frac{\lambda_1^3 2\lambda_2 + 5\lambda_2^2 h_1}{2h_1 - \lambda_1^3} \end{cases} \quad (39)$$

where $\eta_1 > 0, h_1 = \lambda_1(\frac{1}{2}\lambda_1^2 + \lambda_3 - \lambda_1)$ are constants. Finally, sliding mode control input reaches and moves to the sliding surface in finite convergence time as follows equations

$$t_s = \frac{q_1}{\alpha_1(q_1 - p_1)} \ln \frac{\alpha_1 e(0)^{(q_1 - p_1)/q_1} + \alpha_2}{\alpha_2} \quad (40)$$

$$t_r \leq \frac{2}{\gamma_1} \ln \frac{\gamma_1 V_1^{1/2}(0) + \gamma_2}{\gamma_2} \quad (41)$$

t_s and t_r are move time and reaching time to sliding surface [35]. Total finite convergence time is as follows

$$t_c = t_r + t_s \quad (42)$$

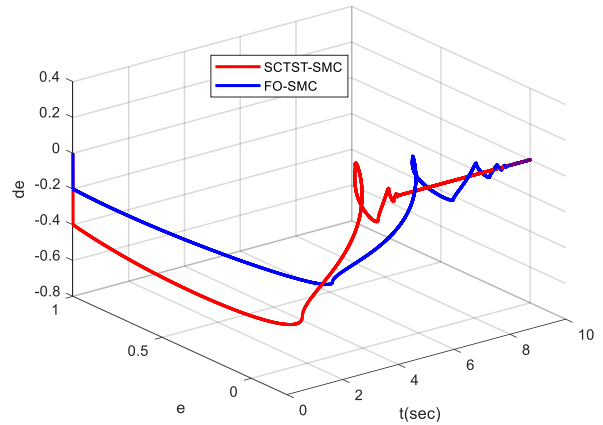


Figure 1. FO-SMC and SCTST-SMC convergence speed on sliding surface graphs

In Figure 1, the graph illustrates the convergence rate of error and error changes over time for both the proposed controller and the traditional sliding mode controller. In this context, when there is an instantaneous reference change and the system is subjected to disturbances, a more effective dynamic response is achieved in speed control.

2.3.1. Control Scheme and Experimental Setup

Two loops, one outer loop speed controller and two inner loop current controllers, make up the cascaded closed

loop PMSM control system. SMC controller is used for constructing the outer loop speed controller, whereas proportional-integral (PI) controllers are used for the inner

loop current controllers. Fig. 2 shows the PMSM's simplified control scheme.

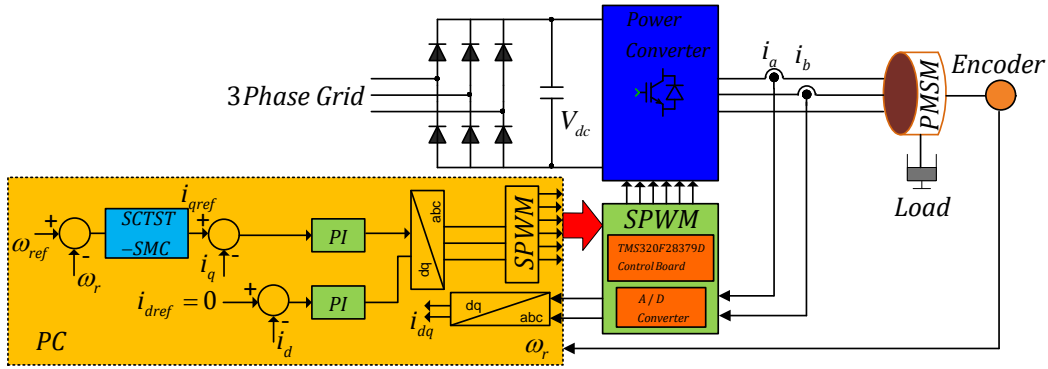


Figure 2. PMSM cascaded control scheme.

The Permanent Magnet Synchronous Motor (PMSM), with a nameplate rating of 0.4 kilowatts, 1.27 Newton meters, and a speed of 3000 revolutions per minute, is powered by a voltage source converter. The motor operates with a phase-to-phase voltage of 200 volts root mean square (Vrms) and a current of 2.7 amperes root mean square (Arms). The electrical characteristics and control settings are detailed in Table I, while the experimental setup is depicted in Fig. 3. The test configuration comprises a TMS320F28379D microcontroller, a current and voltage measurement card, an inverter equipped with IXYS IGBTs, and a PMSM test arrangement. The controller's current loop has a bandwidth of 200 Hz, while the speed loop has a bandwidth of 20 Hz. The operation period of the speed loop is equal to 10 times the period of the carrier signal. To validate the proposed ST-SMC and compare the proposed method with conventional ST-SMC, experiments are carried out in steady-state and transient operations in the relatively low and medium-speed range. In the comparison of the graphs, dynamic features such as reduction of overshoot, fast convergence and disturbance removal are taken into account in the speed response behavior.

Table 1. Motor and controller parameters.

Motor Parameters	Value
Phase Resistance [Ω]	2.5
d,q axis Inductance [H]	$6.5e^{-3}$
Number of Pole Pair	4
V_{ll} [V]	200
Magnet Flux	0.068
Inertia (kgm^2)	$0.31e^{-5}$
Torque Constant (Nm/A)	0.564

3. Experimental Results and Discussion

In the experimental studies, step reference speeds of 250, 750 and 1500 rpm were applied to all three controllers. At the same time, the load torque, which is an external disturbance effect, was applied instantaneously to the PMSM for all three controllers. The results of all three experiments are shown in speed and current graphs. Finally, the graphs of all the controllers are compared in the same graph. All of the experimental results are initialised at 40 seconds as it takes a certain amount of time to embed, compile and run the programme in the DSC. This time also includes the initialisation of the PMSM to the start position, i.e. the alignment position. All graph values were recorded in real-time and transferred to the computer. The load torque was applied to the system at the 50th second with the help of a solid-state relay.

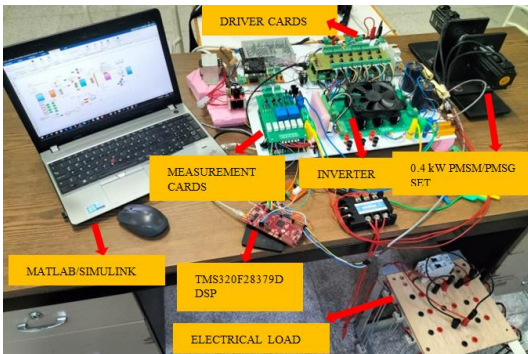


Figure 3. PMSM Experimental Setup Photo.

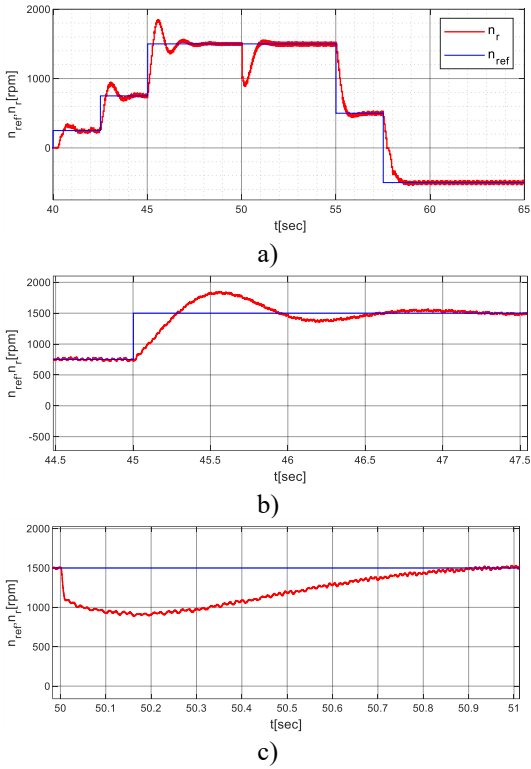


Figure 4.a,b,c) The step response in PMSM speed change for PI control

The dynamic speed responses of the PI controller are exhibited in Figures 4,a,b,c for step reference speed values of 250,750, and 1500 rpm. A comparison table between controller responses is provided after the graphs, indicating the overshoot values in the step reference case and undershoot values in the load torque application scenario.

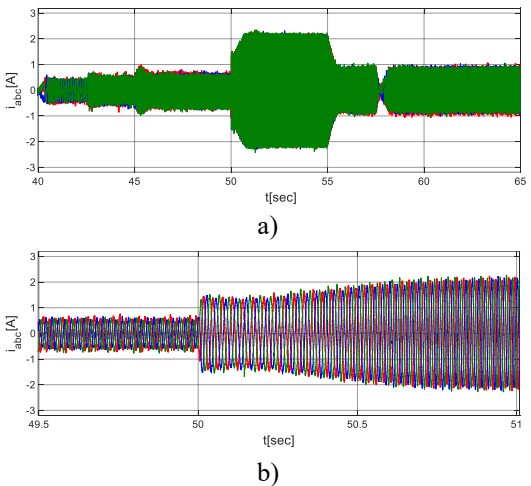


Figure 5.a,b) Three-phase current for PI control

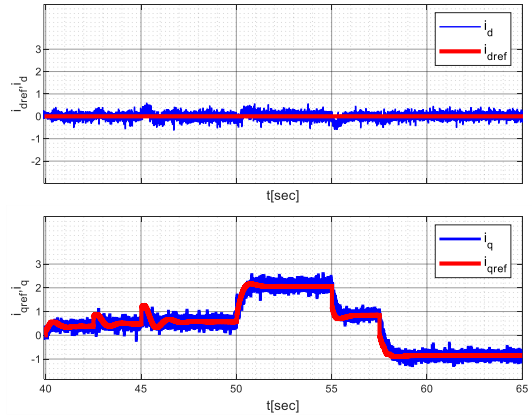


Figure 6. i_{dq} axis currents for PI control

Figures 5 and 6 show the three-phase current graphs and the reference and feedback currents of the dq axes. The reference dq currents are tracked by the feedback currents. No steady-state error is observed.

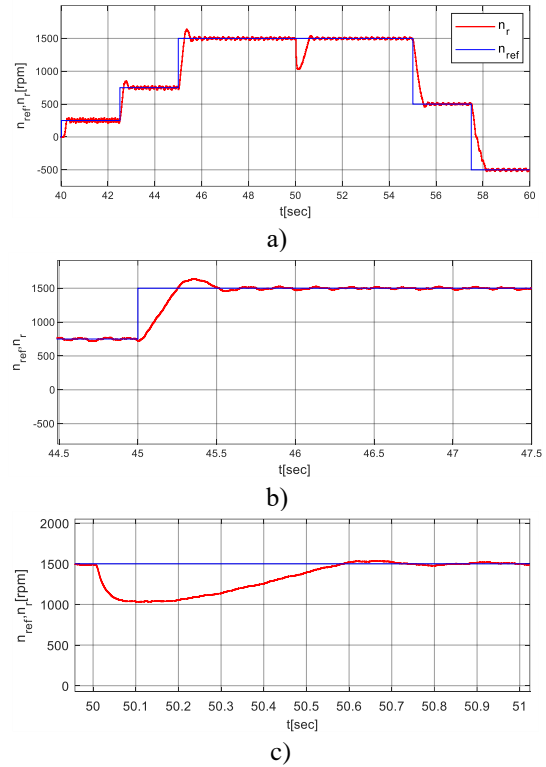


Figure 7. a, b, c) The step response in PMSM speed change for conventional ST-SMC control

Figure 7. a, b, and c illustrate the conventional super-twisting controller speed loop responses. Response to step references and instantaneous load torque is improved in terms of time and value compared to the PI controller. Step response has been substantially improved in terms of overshoot.

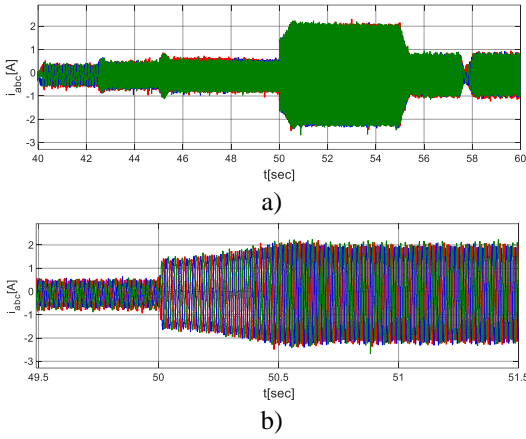


Figure 8. a,b) Three-phase current for conventional ST-SMC control

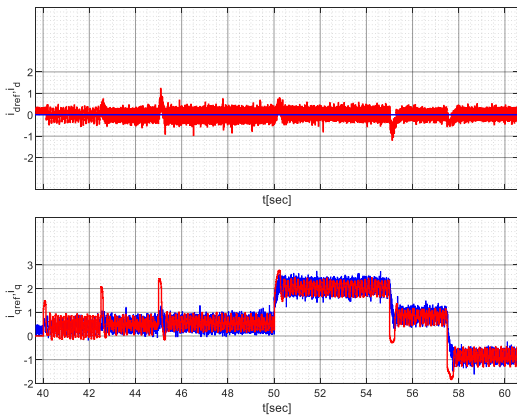


Figure 9. i_{dq} axis currents for conventional ST-SMC control respectively

Figures 8 and 9 show the phase currents in control, as well as the reference and feedback values of the direct and quadrature axis currents. When compared to Figures 5 and 6, the presence of the chattering effect, which is characteristic of sliding mode control, is observed. Additionally, in terms of control response, a more dynamic response is seen compared to the PI controller.

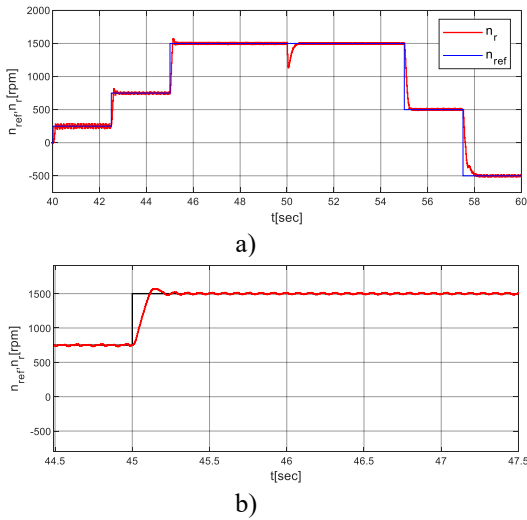


Figure 10. a,b,c) The step response in PMSM speed change for SCTST-SMC control

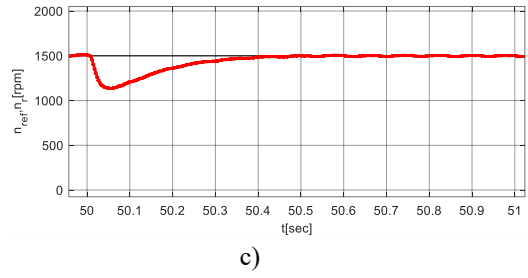


Figure 10. (Cont.) a,b,c) The step response in PMSM speed change for SCTST-SMC control

Figures 10 a, b, and c display the speed responses of the proposed SCTST-SMC controller to different step references, both in general and explicit form. It can be observed that, compared to the traditional PI and sliding mode controllers shown in previous graphs, the SCTST-SMC controller produces a much more dynamic response that meets the control criteria. A comparison of the speed dynamic responses for all controllers will be provided below.

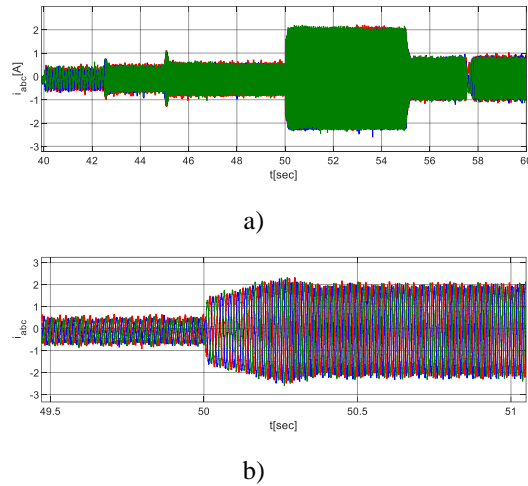


Figure 11.a,b) Three-phase current for SCTST-SMC control

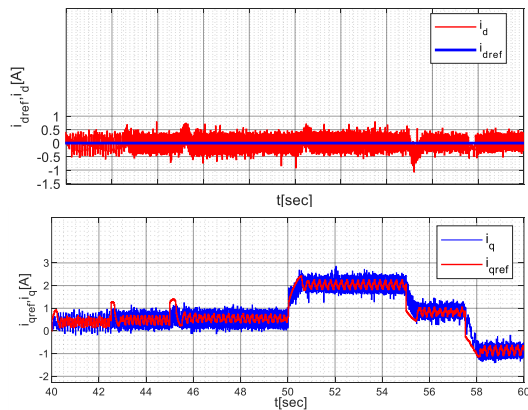


Figure 12. i_{dq} axis currents for SCTST-SMC control respectively

Figures 11 and 12 show the phase currents of the PMSM, as well as the direct and quadrature axis currents, respectively. Compared to the case with traditional sliding mode control, it is observed that the chattering effect is reduced due to the continuous response of the super twisting controller.

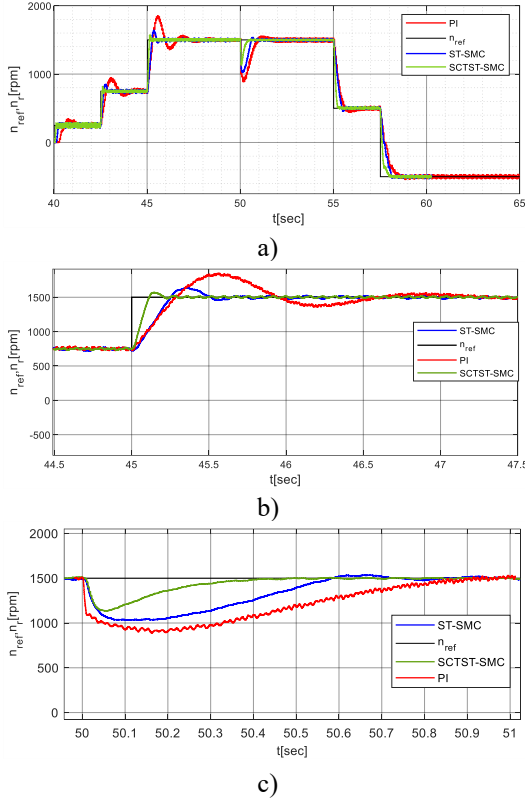


Figure 13.a,b,c) The step response in PMSM speed change for PI, ST-SMC and SCTST-SMC control

The graphs in Figures 13a, b, and c compare the PI, ST-SMC, and SCTST-SMC controllers. The performance of the controllers is clearly illustrated based on the previously applied reference values. The proposed controller demonstrates excellent dynamic response with almost zero overshoot. When a sudden load torque is applied, the proposed controller exhibits superior dynamic behavior, with the lowest dip value compared to the others and a rapid recovery from the load torque impact.

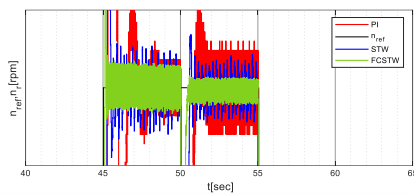


Figure 14. Output speed fluctuations

3.1. Comparative Performance Interpretations

Table 2. Controller performance indicators

Control Method	No Load Operation			Add Load Torque Operation		
	Rise Time (s)	Settling Time (s)	Overshoot (rpm)-%	Rise Time (s)	Settling Time (s)	Under-shoot (rpm)-%
PI	0,27	2,13	1850-%23	50,7	51	895-%40
ST-SMC	0,22	1,25	1620-%8	50,5	50,8	1100-%26,6
SCTST-SMC	0,1	0,42	1560-%4	50,2	50,4	1240-%17,3

Table 2 presents a comparison of the performance indicators for three methods used in PMSM control. In this table, the values for the rise time, settling time, overshoot in no-load condition, and speed drop in loaded condition are clearly shown for the proposed method. Additionally, in terms of the undesirable characteristics of sliding mode controllers, the proposed super-twisting method exhibits less chattering. Thus, both motor control performance and the reduction of chattering have been improved. All loading experiments were conducted through the PMSG generator to correspond to the rated load torque value of approximately 1.27 Nm-1500 rpm. Instantaneous loading was achieved by connecting the load via a precise solid-state relay, which switches the load into the circuit. This allowed the voltage and current generated by the PMSG to be instantly transferred to the resistive load. The diagram of the output speed fluctuation can be seen in Figure 14. Accordingly, the controller output with the least speed fluctuation and thus the chattering effect is the SCTST-SMC controller.

4. Conclusions

From the perspective of convergence trajectory analysis, the presence of system disturbance results in a lag in convergence, which eventually gives rise to a deterioration in dynamic performance. On the other hand, the analyzed SCTST-SMC can successfully counteract any disruptions in the system. This allows the system's state to follow the desired convergence trajectory with no delays in reaching the desired state. The efficacy of the suggested control strategy was validated on the industrial-scale 400 W PMSM platform. The results demonstrated that the analyzed scheme can significantly enhance the system's tolerance to disturbances and its performance during transient periods. Additionally, the PMSM parameters exhibit a high level of robustness as compared to the PI and conventional sliding mode controllers. Future research will primarily focus on developing online optimization research chattering effect alleviating for regulating the velocity of a PMSM motor.

Declaration of Ethical Standards

The author(s) of this article declare that the materials and methods used in this study do not require ethical committee permission and/or legal-special permission.

Conflict of Interest

The authors declare that they have no known competing financial interests or personal relationships that could have appeared to influence the work reported in this paper.

References

- [1] Bartolini, G., Punta, E., & Zolezzi, T. 2007. Approximability properties for second-order sliding mode control systems. *IEEE Transactions on Automatic Control*, **52**(10),pp. 1813–1825.
- [2] Bartoszewicz, A., & Lesniewski, P. 2016. New Switching and Nonswitching Type Reaching Laws for SMC of Discrete Time Systems. *IEEE Transactions on Control Systems Technology*, **24**(2), pp. 670–677.
- [3] Bramerdorfer, G., Winkler, S. M., Kommenda, M., Weidenholzer, G., Silber, S., Kronberger, G., Affenzeller, M., & Amrhein, W. 2014. Using FE calculations and data-based system identification techniques to model the nonlinear behavior of PMSMs. *IEEE Transactions on Industrial Electronics*, **61**(11),pp. 6454–6462.
- [4] Chatri, C., Ouassaid, M., Labbadi, M., & Errami, Y. 2022. Integral-type terminal sliding mode control approach for wind energy conversion system with uncertainties. *Computers and Electrical Engineering*, **99**(January),pp 107775.
- [5] Gonzalez, T., Moreno, J. A., & Fridman, L. 2012. Variable gain super-twisting sliding mode control. *IEEE Transactions on Automatic Control*, **57**(8),pp. 2100–2105.
- [6] Jiang, Y., Xu, W., Mu, C., & Liu, Y. 2018. Improved deadbeat predictive current control combined sliding mode strategy for PMSM drive system. *IEEE Transactions on Vehicular Technology*, **67**(1),pp. 251–263.
- [7] Junejo, A. K., Xu, W., Mu, C., Ismail, M. M., & Liu, Y. 2020. Adaptive Speed Control of PMSM Drive System Based a New Sliding-Mode Reaching Law. *IEEE Transactions on Power Electronics*, **35**(11), pp.12110–12121.
- [8] Kumari, K., Chalanga, A., & Bandyopadhyay, B. 2016. Implementation of Super-Twisting Control on Higher Order Perturbed Integrator System using Higher Order Sliding Mode Observer. *IFAC-PapersOnLine*, **49**(18), pp. 873–878.
- [9] Lascau, C., Boldea, I., & Blaabjerg, F. 2013. Super-twisting sliding mode control of torque and flux in permanent magnet synchronous machine drives. *IECON 2013 - 39th Annual Conference of the IEEE Industrial Electronics Society*, Vienna, Austria, pp. 3171-3176.
- [10] Lee, S. B. 2006. Closed-loop estimation of permanent magnet synchronous motor parameters by PI controller gain tuning. *IEEE Transactions on Energy Conversion*, **21**(4), pp. 863–870.
- [11] Levant, A. 1993. Sliding order and sliding accuracy in sliding mode control. *International Journal of Control*, **58**(6), pp.1247–1263.
- [12] Li, K., Bouscayrol, A., Cui, S., & Cheng, Y. ,2021. A Hybrid Modular Cascade Machines System for Electric Vehicles Using Induction Machine and Permanent Magnet Synchronous Machine. *IEEE Transactions on Vehicular Technology*, **70**(1), pp. 273–281.
- [13] Li, Y., & Xu, Q. ,2010. Adaptive sliding mode control with perturbation estimation and PID sliding surface for motion tracking of a piezo-driven micromanipulator. *IEEE Transactions on Control Systems Technology*, **18**(4), pp. 798–810.
- [14] Linares-Flores, J., García-Rodríguez, C., Sira-Ramírez, H., & Ramírez-Cárdenas, O. D. , 2015. Robust Backstepping Tracking Controller for Low-Speed PMSM Positioning System: Design, Analysis, and Implementation. *IEEE Transactions on Industrial Informatics*, **11**(5),pp. 1130–1141.
- [15] Liu, M., Chan, K. W., Hu, J., Xu, W., & Rodriguez, J., 2019. Model Predictive Direct Speed Control With Torque Oscillation Reduction for PMSM Drives. *IEEE Transactions on Industrial Informatics*, **15**(9), pp. 4944–4956.
- [16] Liu, X., & Yu, H. ,2021. Continuous adaptive integral-type sliding mode control based on disturbance observer for PMSM drives. *Nonlinear Dynamics*, **104**(2), pp.1429–1441.
- [17] Mao, D., Wang, J., Tan, J., Liu, G., Xu, Y., & Li, J. ,2019. Location Planning of Fast Charging Station Considering its Impact on the Power Grid Assets. *2019 IEEE Transportation Electrification Conference and Expo (ITEC)*, Detroit, MI, USA,pp. 1-5.

- [18] Moreno, J. A., & Osorio, M., 2008. A Lyapunov approach to second-order sliding mode controllers and observers. 2008 47th IEEE Conference on Decision and Control, Cancun, Mexico, 2008, pp. 2856-2861
- [19] Muñoz, F., Bonilla, M., González-Hernández, I., Salazar, S., & Lozano, R., 2015. Super Twisting vs Modified Super Twisting algorithm for altitude control of an Unmanned Aircraft System. 2015 12th International Conference on Electrical Engineering, Computing Science and Automatic Control (CCE), Mexico City, Mexico, pp. 1-6
- [20] Nguyen, N. P., Oh, H., & Moon, J., 2022. Continuous Nonsingular Terminal Sliding-Mode Control with Integral-Type Sliding Surface for Disturbed Systems: Application to Attitude Control for Quadrotor UAVs under External Disturbances. IEEE Transactions on Aerospace and Electronic Systems, **58**(6), pp. 5635–5660.
- [21] Ouledali, O., Meroufel, A., Wira, P., & Bentouba, S., 2015. Direct Torque Fuzzy Control of PMSM based on SVM. Energy Procedia, **74**, pp.1314–1322.
- [22] Pisu, P., & Rizzoni, G., 2007. Strategies for Hybrid Electric Vehicles. IEEE Transaction on Control System Technology, **15**(3), pp. 506–518.
- [23] Samaranyake, L., & Longo, S., 2018. Degradation Control for Electric Vehicle Machines Using Nonlinear Model Predictive Control. IEEE Transactions on Control Systems Technology, **26**(1), pp. 89–101.
- [24] Savitski, D., Ivanov, V., Augsburg, K., Emmei, T., Fuse, H., Fujimoto, H., & Fridman, L. M., 2020. Wheel Slip Control for the Electric Vehicle with In-Wheel Motors: Variable Structure and Sliding Mode Methods. IEEE Transactions on Industrial Electronics, **67**(10), pp. 8535–8544.
- [25] Shtessel, Y. B., Moreno, J. A., Plestan, F., Fridman, L. M., & Poznyak, A. S., 2010. Super-twisting adaptive sliding mode control: A Lyapunov design. 49th IEEE Conference on Decision and Control (CDC), Atlanta, GA, USA, pp. 5109-5113.
- [26] Stojic, D. M., Milinkovic, M., Veinovic, S., & Klasnic, I., 2015. Stationary Frame Induction Motor Feed Forward Current Controller with Back EMF Compensation. IEEE Transactions on Energy Conversion, **30**(4), pp. 1356–1366.
- [27] Teja, A. V. R., Chakraborty, C., & Pal, B. C., 2018. Disturbance Rejection Analysis and FPGA-Based Implementation of a Second-Order Sliding Mode Controller Fed Induction Motor Drive. IEEE Transactions on Energy Conversion, **33**(3), pp. 1453–1462.
- [28] Wang, B., Dong, Z., Yu, Y., Wang, G., & Xu, D., 2018. Static-Errorless Deadbeat Predictive Current Control Using Second-Order Sliding-Mode Disturbance Observer for Induction Machine Drives. IEEE Transactions on Power Electronics, **33**(3), pp. 2395–2403.
- [29] Wang, G., Liu, R., Zhao, N., Ding, D., & Xu, D., 2019. Enhanced Linear ADRC Strategy for HF Pulse Voltage Signal Injection-Based Sensorless IPMSM Drives. IEEE Transactions on Power Electronics, **34**(1), pp. 514–525.
- [30] Wang, Y., Feng, Y., Zhang, X., & Liang, J., 2020. A New Reaching Law for Antidisturbance Sliding-Mode Control of PMSM Speed Regulation System. IEEE Transactions on Power Electronics, **35**(4), pp. 4117–4126.
- [31] Wang, Y., Zhu, Y., Zhang, X., Tian, B., Wang, K., & Liang, J., 2021. Antidisturbance Sliding Mode-Based Deadbeat Direct Torque Control for PMSM Speed Regulation System. IEEE Transactions on Transportation Electrification, **7**(4), pp. 2705–2714.
- [32] Xu, B., Zhang, L., & Ji, W., 2021. Improved Non-Singular Fast Terminal Sliding Mode Control with Disturbance Observer for PMSM Drives. IEEE Transactions on Transportation Electrification, **7**(4), pp. 2753–2762.
- [33] Young, K. D., Utkin, V. I., & Özgüner, Ü., 1999. A control engineer's guide to sliding mode control. IEEE Transactions on Control Systems Technology, **7**(3), pp. 328–342.
- [34] Zhang, Y., McLoone, S., Cao, W., Qiu, F., & Gerada, C., 2017. Power Loss and Thermal Analysis of a MW High-Speed Permanent Magnet Synchronous Machine. IEEE Transactions on Energy Conversion, **32**(4), pp. 1468–1478.
- [35] Zhang, Z., Ma, R., Wang, L., & Zhang, J., 2018. Novel PMSM Control for Anti-Lock Braking Considering Transmission Properties of the Electric Vehicle. IEEE Transactions on Vehicular Technology, **67**(11), pp. 10378–10386.